

Physically-based Thermal Simulation of Large Scenes for Infrared Imaging

B. Kottler, E. Burkard, D. Bulatov and L. Haraké

*Department of Scene Analysis, Fraunhofer Institute of Optronics, System Technologies and Image Exploitation (IOSB),
76275 Ettlingen, Germany*

Keywords: Physics-Based, Thermal Infrared, Heat Simulation, Heat Transfer Modeling, Finite Volume Method.

Abstract: Rendering large scenes in the thermal infrared spectrum requires the knowledge of the surface temperature distribution. We developed a workflow starting from raw airborne sensor data yielding to a physically-based thermal simulation, which can be used for rendering in the infrared spectrum. The workflow consists of four steps: material classification, mesh generation, material parameter assignment, and thermal simulation. This paper concerns the heat transfer simulation of large scenes. Our thermal model includes the heat transfer types radiation, convection, and conduction in three dimensions within the object and with its environment, i.e. sun and sky in particular. We show that our model can be solved by finite volume method and it shows good agreement with experimental data of the CUBI object. We demonstrate our workflow for sensor data from the City of Melville and produce reasonable results compared to infrared sensor data. For the large scene, the temperature simulation finished in appropriate time of 252 sec. for five day-night cycles.

1 INTRODUCTION AND PREVIOUS WORK

1.1 Motivation

Thermal simulation of large scenes is essential when it comes to applications like meteorology, assessment of atmospheric pollution, camouflage evaluation in the military applications or detection of urban heat islands and corresponding heat radiation for city planners. All these applications and especially the last one have a strong dynamic component, since to the same extent as augmentation of both the global earth temperature rises, so does urbanization degree.

From the point of view of a city planner, whose job is to respond to the needs of the later generations without putting upside down the infrastructure needed for the current one, the ability to render large three-dimensional scenes in thermal infrared wavelength spectrum is a very interesting aspect. In which distances along the roads should the trees be planted and which kinds of trees should actually be used to reduce the heat radiation to an acceptable amount? Which heights and roof materials for the public buildings are least susceptible to the appearance of urban heat islands? Fast and reliable scene rendering in thermal infrared allows assessing the long-term energy bal-

ance for these scenarios. The temperature of the surface should be ideally modeled as a function of the current atmospheric condition, surface geometry and material composition, socio-economic situation, and many others. Of course, a city planner cannot start from scratch, but must deal with the existing realities, or initial conditions. For a more precise simulation of temporal development of the surface temperature and subsequent thermal rendering, the main requirement is to know as much as possible about the surface. Here it is often not enough to use the existing geographical data, because they may be obsolete or just lack some relevant information, such as building roof materials and roof forms.

To be able to free ourselves from too many input requirements (accurate 3D models, numerous temperature measurements), we are currently designing an end-to-end pipeline starting at raw airborne sensor data and yielding semantic and three-dimensional environments rendered in thermal infrared. The focus of this paper will concern the simulation of the surface temperature of large scenes. This may not only be used directly in many applications but also is basic for thermal rendering, i.e., determining the heat radiance since every object having a temperature above absolute zero radiates at infrared wavelengths. The reason to utilize the airborne data is that

large parts of the scene are captured and the measurements of geometry and material classification are actual. From these measurements, there are plenty of previous work achieved on accurate 3D city modeling and material classification (Bulatov et al., 2014; Xiong et al., 2014). The first reason for producing semantic scenes is that land-cover classes and material classes are strongly correlated, e.g. within one building, roofs consist of few materials, trees can be represented by generic models. Otherwise assigning materials to single roof polygons making up the scene and figuring out the emitting properties of these materials are two tedious procedures. The second reason is that once these models are available, further important data, such as material composition of building walls or analysis of socio-economic developments are easier to integrate. A particular challenge for the geometry component of the above module is the complexity of the underlying scene. Besides, shadow cast is a crucial component for surface temperature, which cannot be employed in 2D case (Dewan and Corner, 2014). Finally, to provide an accurate ground truth measurement in closest-range three-dimensional scenarios, which are appropriate for detecting urban heat islands, among others, an efficient rendering routine can replace numerous punctual measurements of temperatures and provide a glance into the future by means of simulation. The complexity of the problem is the reason why there are only a few publications focused on simulation of surface temperature in larger three-dimensional environments, as we will see in the remainder of this section. Also, we will see that (Xiong et al., 2016) is the most similar contribution to our work, however, there are still several differences and improvements it is worth being focused on.

1.2 Previous Approaches

We start our short literature review by 2D-based approaches. Essentially, convection and emission equations are retrieved from land-cover/material classification results (Bartos and Stein, 2015; Feng and Myint, 2016; Dewan and Corner, 2014). Three-dimensional scene elements are treated by unfolding; hence, effects of shadow cast remain unconsidered. However, for close-range applications around selected monuments, the surrounding 3D terrain (heights of the trees and buildings) must not be neglected and thus the challenge is to combine the automatic urban terrain reconstruction and thermal simulation. A well-established software MuSES, designed for the US army, is introduced in (Johnson et al., 1998). In particular, it shows how the level of automatization in thermal simulation was increased with

respect to the previous system. The remaining interactive parts were on the one hand uploading the 3D geometry and assigning material properties, and on the other hand, quality control since the system was presumably used for camouflage and deception. It becomes clear that an automatic creation of 3D models assigned with material properties is tempting for a more rapid progress in the field. The authors of (Lagouarde et al., 2010) are more interested in measuring temperatures from different viewing directions since it correlated with radiation emitted by an ensemble of structure. In the first part of their work, they assess directional anisotropy that is the difference between the directional and the nadir temperatures. In the second part of the work, the model at a given direction is rendered and the aggregated directional temperature at a given pixel is obtained using the classes and the raw values for the surface temperature from the first step. While the 3D models were provided from the public sources, the authors only made a difference between six configurations, that is two light settings (sunlit or shaded) and the three land-cover classes (roof, wall, and soil with materials assigned more or less arbitrarily). Performing the three-dimensional aggregation of temperatures is another critical generalization of their method. The advanced treatment of shadows is described in (Poglio et al., 2002). The authors adaptively subdivide the triangles in illuminated and shaded ones, ensuring that the new triangles are not degenerated. As for development of the simulated scene over time, they refer to (Johnson et al., 1998). A summary of the physics of heat transport in large scenes can be found in (Maréchal et al., 2010). In their voxel-based approach, a method for simulating realistic winter appearance based on a physical simulated temperature distribution for alpine regions is presented. For us this paper gives a good overview about components of our simulation.

Most similar to our contribution is (Xiong et al., 2016). From raw meshes, classification of triangles into ground, vegetation, building wall and building roof takes place using simple 3D-based features (elevation, planarity, and horizontality) and Markov Random Fields. In the next steps, the portions of the mesh corresponding to buildings are modeled as water-tight multi-planar structure while the remaining elevated portions of the mesh are ignored. For every mesh element, heat balance equation comprising terms for radiation, conduction, and convection is solved. The shadows are taken into account as well in the radiation term. This pioneering work can be questioned in two aspects. First, the raw meshes were created from images by means of structure from motion procedures. However, the images were not considered for assign-

ing material properties to surface triangles. The second problem is that the vegetation was not considered even though presence of trees is very valuable for reducing the urban heat.

1.3 Contributions

Our improvements will include land-cover classification from combined image- and point-based features. From the image based classification result, we triangulate the terrain using Restricted Top-Down Quadree Triangulation (Pajarola, 2002). The triangulated terrain has three important properties: memory efficiency, accuracy, and consistence.

To this terrain mesh, we add the building models. For this contribution, we will use the terms land-cover and material classification synonymous, assuming, for example, that the building roofs and walls are comprised by two uniform materials. Contributions achieving a more detailed subdivision of building roofs into materials using multi-spectral and high-resolution images exist in the literature (Ilehag et al., 2018) and thus our approach can be easily extended. Besides, we detect high vegetation and add trees to the mesh as well, currently modeled in the shape of forest boxes, i.e. trees standing close to each other are merged and single trees are disregarded. Furthermore, we are able to take shadows into account as the simulation is performed on a surface embedded in the 3-dimensional space and thus includes occlusion analyses.

A physical approach was chosen to calculate the surface temperatures with the heat equation. This is a partial differential equation, i.e. it includes spatial and temporal derivations. For the temporal derivations, the forward Euler integration was used. The spatial derivations were discretized with a finite volume method. For this purpose, the simulation area is divided into finite volumes and the flows on the boundaries of the volumes are evaluated. We will consider ten classes in total and for each of these classes, we derive the necessary coefficients from the literature.

In this paper, we propose a framework for simulating realistic temperature distributions for large sceneries. This is the core aspect of a complex workflow from sensor data to semantic urban terrain models rendered in thermal spectrum.

2 PRELIMINARIES

Since the focus of this paper concerns the temperature simulation step of the pipeline, or the bottom block of

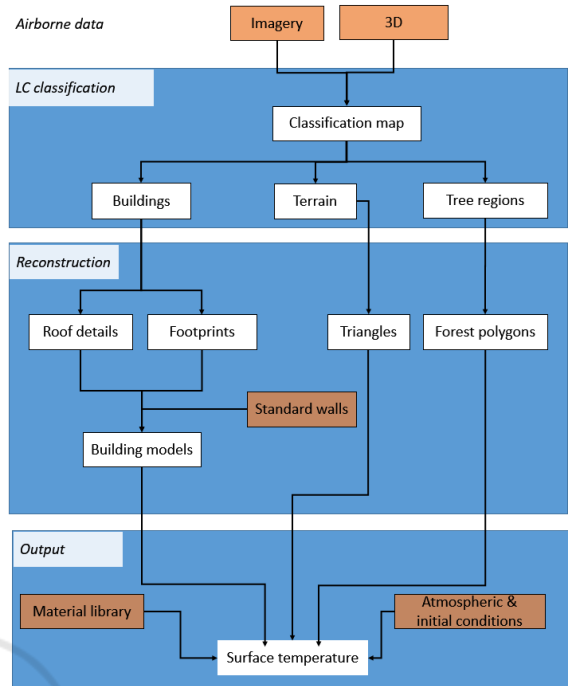


Figure 1: Pipeline – From Sensor to Surface Temperature.

Figure 1, we decided to give a short summary of the physical background necessary for thermal simulation and how it states the basis for infrared rendering, as well as the preceding steps leading from raw airborne data to a semantic 3D representation of the scene.

2.1 Infrared Rendering and Physical Background of Thermal Flow

Starting with the Kajiya’s well-known rendering equation, cp. (Kajiya, 1986),

$$L(x, \vec{\omega}) = L_e(x, \vec{\omega}) + L_r(x, \vec{\omega}), \quad (1)$$

with the total radiance $L(x, \vec{\omega})$ from surface point x in direction $\vec{\omega}$ which consists of the emitted radiance L_e and the reflected radiance from the upper hemisphere of the surface L_r , we have to take into account the temperature dependence of the emissive radiation term L_e if regarding the thermal spectrum for rendering,

$$L_e(x, \vec{\omega}) = L_e(x, \vec{\omega}, T), \quad (2)$$

where T is the surface temperature at point x . In order to evaluate this equation and render an arbitrary scene in the infrared spectrum, one has to know the surface temperature at every observed point in the scene. However, temperature is not a property as color or texture, but depends on the environment, time of the day, physical material parameters, temperature history, and so on. Determining the surface temperature

of a scene at a specific point in time requires the simulation of heat transfer.

In general, heat transfer follows the first law of thermodynamics where we will consider constant volumes,

$$mC_v \frac{dT}{dt} = Q \quad (3)$$

with the mass m , the specific heat capacity C_v at constant volume, the temperature T and the heat transfer rate Q per unit area (Lienhard IV and Lienhard V, 2011). This rate is compound by the three modes of heat transfer: radiation, conduction and convection. For the sake of completeness, it shall be pointed out that heat can also be chemically stored in the form of latent heat caused by phase change, e.g. vaporization. However, this will not be included in the thermal model presented in this paper.

Heat conduction takes place predominantly within solids and fluids, and the conductive heat transfer follows Fourier's law,

$$mC_v \frac{dT}{dt} = K \Delta T \quad (4)$$

with the thermal conductivity K . Convection involves the surrounding medium, e.g. the air in an urban area. Free convection describes the phenomenon of a medium being heated or cooled by a surface and therefore starting to move. Forced convection refers to an already moving medium, e.g. due to wind, exchanging heat with a surface. The convective heat transfer depends on the difference between the surface temperature T and the surrounding medium's temperature T_{medium} ,

$$mC_v \frac{\partial T}{\partial t} \propto T - T_{\text{medium}}. \quad (5)$$

Regarding radiative heat transfer, all matter with a temperature greater than absolute zero emits thermal radiation. For a blackbody, which is defined by absorption and re-emission of all incoming light, the radiation power follows the Stefan-Boltzmann law, $P = \sigma T^4$ with the Stefan-Boltzmann constant σ , and the temperature T (Siegel and Howell, 1992). With the so-called grey-body approach, the actual radiative power is given by a constant fraction of a blackbody's radiative power, defined by the emissivity $\epsilon \in [0, 1]$, where $\epsilon = 1$ equals a blackbody. In estimating the balance heat transfer in a scene with several objects, one has to model the heat radiation of each object and taking into account the mutual visibility. This is where the 3D geometry of the scene becomes indispensable. With sun and sky as main participants, the challenge is to efficiently perform shadow analysis.

Figure 2 shows an overview of the types of the modeled thermal phenomena.

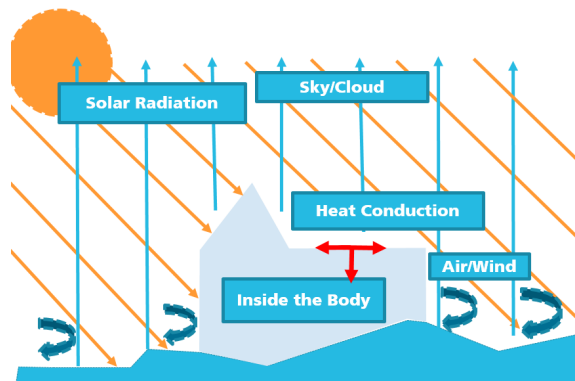


Figure 2: Overview of the considered physical phenomena in the thermal simulation.

2.2 From Sensor Data to Semantic Surface Representation

The semantic reconstruction and material classification are important preprocessing steps, since the heat simulation depends strongly on the material properties and geometry, as mentioned above.

We assume the availability of the elevation data, sampled into DSM (Digital Surface Model). Combining image and elevation data, land-cover classes are obtained. Hereby, the building class is particularly important for the subsequent 3D modeling step, since buildings as man-made objects are heated or cooled from the inside, or roof materials are generally different. Other important classes are: bare soil, grass, tree, water and road. Various approaches exist for land-cover classification. We are interested in ones which need only a few training patches and features. Therefore, we opted for a conventional approach based on Random Forests classifier (Breiman, 2001). As image-based features, we took the channels of the multispectral image, vegetation and water indices. As elevation-based features, we considered relative elevation, whereby a standard interpolation procedure was chosen to reconstruct the ground, as well as the planarity measure (Gross and Thönnessen, 2006). Training patches were sampled interactively. After building detection, (Bulatov et al., 2014) suggest performing their delineation (for simplification of shapes), outlining and roof detail reconstruction. However, building models resulting from such a data-driven approach are not water-tight, causing problems for the simulations. Therefore and because in our data set, the buildings are not too high, for this work, we decided to use the freely available shapefile with building outlines and to model every building as a prismatic structure with elevation retrieved from sensor data. Building walls are modeled as vertical trapezoids by projecting the endpoints of border- or step-

edges of the roof to the ground. For the tree regions, we will concentrate on large forest regions. They are represented as *forest boxes* and allow to model huge forest areas by at most several dozens of polygons (Decaudin and Neyret, 2004; Häufel et al., 2017). The last data preparation step concerns meshing of the terrain. Starting at the classification result, we wish to assign a class to every triangle. Therefore, after several morphological operations allowing to suppress too small regions, we consider a canonical rectangular grid along the axes x and y . Tracing one diagonal of each rectangle in the grid as well as assigning the ground values of vertices as z coordinates results in a coarse triangle mesh. In the initial mesh, those triangle with either elevation or class discontinuities can be subdivided along their symmetry axis into a pair of smaller triangles. In order to avoid cracks in the final surface (that result if a 2D mesh vertex is an inner point of an edge, because the corresponding 3D point is not necessarily incident with the an edge connecting the 3D endpoints of this edge), adjacent triangles must be subdivided as well and, sometimes, new vertices must be inserted. This approach was referred in (Pajarola, 2002) as *restricted (top-down) quadtree triangulation* (RQT or RTDQT) and was implemented in this work.

3 MODELING THERMAL TRANSFER

In this section, we present our architecture for simulating thermal transfers for large sceneries, whose geometry is determined by a surface model. First, the data representation and our simulation basis referred to as surface volume are introduced. Furthermore, we give an overview of the considered physical parameters of one surface volume element and the environmental model as well as the core equation for the implementation. Finally, a mathematical description of the considered physical modes of heat transfer is given.

3.1 Data Representation and Model Principle

Surface Volume Model: The basis of the simulation is the heat equation, which describes the distribution of heat in a given volume over time. For this, we extend the surface model of the scene to a surface volume by giving the surface a thickness.

There are three types of heat propagation in this volume: the heat can be propagated by conduction

within the volume, there is a heat exchange with the outside world and heat exchange with the inside of the body. Mathematically, the thermal conduction in the surface volume can be described with the heat equation and suitable boundary conditions:

$$C_v \rho \frac{\partial T}{\partial t} = K \Delta T \quad \text{in the interior,} \quad (6)$$

$$T = T_{\text{Core}} \quad \text{on the inner surface,} \quad (7)$$

$$\nabla T \cdot \mathbf{n} = Q \quad \text{on the outer surface,} \quad (8)$$

where \mathbf{n} is the outer normal of the wall surface and the thermal conductivity K of the material. In this model, the inner side of the surface volume interacts only with the inner body, which has an internal temperature T_{Core} assumed to be constant. The core temperature can be used to model socio-economic conditions, such as heated buildings. The outer side interacts with the outer world, where the total heat flow is denoted with Q .

For solving this partial differential equation a finite volume method in 3D is implemented. For this purpose, the surface is discretized with a coarse triangular mesh, which was given a thickness. The finite volume method is based on balancing the thermal energy flux of the triangular prisms.

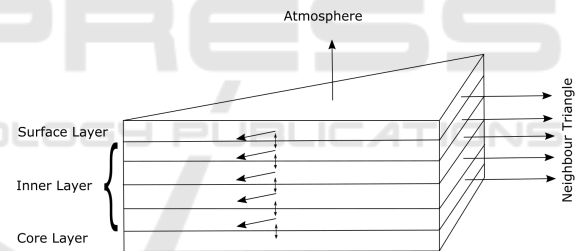


Figure 3: Principle of surface volume discretization.

Model of Geometry and Materials: The basis of the simulation is a triangulated surface mesh representing the geometry of the scene in which the third dimension is implicitly treated. The surface volume model consists of N layers, that means for each triangle overall $2 + N$ temperature values have to be stored: the surface temperature, N temperature values for every layer, and the core temperature (see Figure 3).

Furthermore, every triangle is assumed to consist of one specific material class, which implies a set of parameters representing the physical properties according to Table 1. The parameters can be divided into material properties and environmental properties, the latter ones depend not only on the material but on environmental model and correspond not necessarily to a physical equivalent.

Table 1: Overview of Parameters.

Material Properties	Symbol
Albedo	α
Emissivity	ε
Density	ρ
Specific heat	C_v
Thermal conductivity	K
Thickness of the layers	d_s, d_1, \dots, d_N
Environmental Properties	
Core temperature	T_{Core}
Free convection	h_1
Forced convection	h_2
Wind velocity	v_{wind}
Air temperature	T_{air}
Relative humidity	r_h

Discretization of the Inner Model: The discretization of the model is similar to (Bartos and Stein, 2015) with the difference that we set the parameters using a database and do not need to be fitted. The model of the inner temperature for N layers leads to a system of $N + 1$ coupled differential equations, describing the temperature along the profile of the surface volume.

For the first inner layer we have the equation

$$C_v \rho \frac{\partial T_1}{\partial t} = \frac{K}{d_1} (T_s - 2T_1 + T_2) + K \Delta T_1, \quad (9)$$

for layers with the index $i = 1, \dots, N - 1$, we have

$$C_v \rho \frac{\partial T_i}{\partial t} = \frac{K}{d_i} (T_{i-1} - 2T_i + T_{i+1}) + K \Delta T_i, \quad (10)$$

and for the last inner layer we have

$$C_v \rho \frac{\partial T_N}{\partial t} = \frac{K}{d_N} (T_{N-1} - 2T_N + T_{\text{Core}}) + K \Delta T_N. \quad (11)$$

Model of the Environment: The model for the environment consists of a small set of functions describing the time course of the weather. The weather parameters taken into account are the air temperature $T_{\text{Air}}(t) \in \mathbb{R}$ and relative humidity $r(t) \in [0, 100]$, which can be varied between triangles. Furthermore, the cloud cover is described by $C(t) \in [0, 1]$, where 0 stands for cloud-free sky and 1 for a dense cloud cover. The atmospheric damping is summarized by the factor $I_c(t) \in [0.3, 0.8]$, which is called clearness index. It is defined by $I_c(t) = 0.8 - 0.5C(t)$, cf. (Maréchal et al., 2010). The environmental parameters have to be precalculated from weather data or specified by the user.

Temporal Discretization: For every triangle of the scene the current temperature, material parameters are

stored. The time discretization is performed using a forward Euler integration scheme. Let Δt denote the time step for integration of triangle i . At every time-step n , the total flux Q_i is computed as the sum of all heat fluxes, hence the new temperature is computed as

$$T_i^{n+1} = T_i^n + \frac{Q_i}{\rho_i C_{p_i} A_i d_i} \Delta t, \quad (12)$$

where d_i denotes the thickness of the layer corresponding to the triangle i . The parameter Δt is chosen after a stiffness analysis of the linear system. Numerical experiments have shown that a time step of $\Delta t = 30$ s leads to stable results and records the time-dependent weather phenomena with a good accuracy.

3.2 Physical Modeling of Thermal Flows

In the following, we present the modeling of thermal fluxes, describing the physical phenomena mentioned in Section 2.1 and some details of the numerical implementation.

The thermal change of a surface volume is calculated using the heat equation

$$C_v \rho d_s \frac{\partial T_s}{\partial t} = A + I + D + R + S = Q, \quad (13)$$

where A describes the convective thermal exchange with the surrounding air, I describes the inner model of the surface, D describes the conductive thermal exchange with neighboring triangles, R describes the radiative thermal exchange with the sky, and S describes the thermal flow through direct sunlight. The total flux is denoted with Q . The following deals with the modeling of these fluxes.

3.2.1 Convective Thermal Exchange

The thermal exchange between the surface and the surrounding air is divided into free convection and forced convection whereas we choose a linear model. Let h_1 denote the coefficient for free convection and h_2 the coefficient for forced convection, v_{wind} the wind speed, and T_{Air} the temperature of the air. Then the heat flux between a surface triangle and the air can be described by Newton's law of cooling for free convection and a linear model for forced convection

$$A = (h_1 + h_2 \cdot v_{\text{wind}})(T_{\text{Air}} - T_s). \quad (14)$$

3.2.2 Conductive Thermal Exchange with the Inner Model

Heat conduction dominantly depends on the materials thermal conductivity. Assuming only homogeneous

media and considering only temperature ranges typical for urban sceneries, the thermal conductivity can be assumed constant (Lienhard IV and Lienhard V, 2011). Regarding one-dimensional flow, the surface temperature is coupled to the inner model with the connection

$$I = \frac{K}{d_1}(T_1 - T_s), \quad (15)$$

where d_1 is the discretization parameter defining the surface layers' thickness.

3.2.3 Conductive Thermal Exchange Along the Surface

In addition to conduction into the interior of the body, there is also conduction along the surface. It is calculated with a discretization of the Laplace operator in 2D

$$D = K\Delta T_s. \quad (16)$$

The discretization of the gradient along the surface is done with a finite volume method, where for every face of the triangle the heat flux of the neighboring triangle is calculated. The total flux for a triangle i with the area A_i is then given by

$$(\Delta T)_i \approx \frac{1}{A_i} \sum_{j \in \mathcal{N}_i} L_{ij} (\nabla T)_{ij} \cdot \mathbf{n}_{ij}. \quad (17)$$

where \mathcal{N}_i denotes the set of neighboring triangles of triangle i , $(\nabla T)_{ij}$ the flux, \mathbf{n}_{ij} the outer normal of the edge between triangle i and triangle j , and L_{ij} the length of that edge.

3.2.4 Radiative Thermal Exchange with the Sky

In our model, we assume that a surface triangle can be either oriented to the sky and exchange thermal radiation, or oriented to another surface triangle, which has a similar temperature, so the thermal radiation can be neglected.

In a preprocessing step using OpenGL renderings of the scene with different angles, the visibility of the surface is determined. A rendering is done in two steps. First, the scene is rendered from the perspective of sky and the depth information is stored for each visible object. Then the scene is rendered again, where for each pixel the depth information is used to determine whether it is visible to the sky. If this is the case, the pixel store the index of the corresponding triangle. After a histogram analysis, the portion of the surface of each triangle that is not occluded by other triangles is determined. The visibility of the surface from the viewpoint of the sky is then defined as the mean of all angles and denoted by the parameter $\gamma_{\text{Sky}} \in [0, 1]$.

The temperature of the sky depends on the temperature of the air, the dew point temperature for a cloudless sky and the time of day denoted by $h(t) \in [0, 24]$. The dew point temperature T_{dp} is approximated by the Magnus approximation with the air temperature T_{Air} and relative humidity r through saturation vapour pressure (SVP) and vapour pressure (VP), c.f (Sontag, 1990)

$$\text{SVP}(t) = 6.1078 \cdot 10^{\frac{a \cdot T_{\text{Air}}}{b + T_{\text{Air}}}}, \quad (18)$$

$$\text{VP}(t) = \frac{r}{100} \cdot \text{SVP}, \quad (19)$$

$$T_{\text{dp}}(t) = b \cdot \frac{v(t)}{a - v(t)}, \quad (20)$$

where $v(t) = \log_{10} \left(\frac{\text{VP}(t)}{6.1078} \right)$ and

$$\begin{cases} a = 7.5, & b = 237.3 & \text{for } T_{\text{Air}} \geq 0, \\ a = 7.6, & b = 240.7 & \text{for } T_{\text{Air}} < 0. \end{cases} \quad (21)$$

As in (Maréchal et al., 2010), the temperature of the clear sky is approximated by

$$\begin{aligned} T_{\text{Sky}} &= T_{\text{Air}}(t) \left(0.711 + 0.0056 T_{\text{dp}}(t) \right. \\ &\quad \left. + 7.3 \cdot 10^{-5} T_{\text{dp}}(t)^2 + 0.013 \cos \frac{2\pi h(t)}{24} \right)^{\frac{1}{4}} \end{aligned} \quad (22)$$

The temperature of the clouds is calculated based on the assumption that the air temperature drops 9.84°C and dew point temperature drops 1.82°C per 1000 m of altitude. Then, the height of the clouds can be estimated by

$$H_{\text{cloud}} = (T_{\text{Air}} - T_{\text{dp}}) / (9.84 - 1.82) \cdot 1000. \quad (23)$$

The following equation is used to estimate the clouds' temperature:

$$T_{\text{cloud}} = -0.00182 \cdot H_{\text{cloud}} + T_{\text{dp}}. \quad (24)$$

The total temperature of the cloudy sky is approximated with the weighted mean of the cloud temperature and clear sky temperature, thus

$$T_{\text{total}} = C \cdot T_{\text{cloud}} + (1 - C) T_{\text{sky}}, \quad (25)$$

where C denotes the cloud cover index.

The total thermal flux between a given triangle and the cloudy sky is calculated by the Stefan-Boltzmann law

$$R = \varepsilon \sigma \gamma_{\text{Sky}} (T_{\text{total}}^4 - T_s^4), \quad (26)$$

where ε denotes the emissivity of the material of the triangle.

3.2.5 Thermal Heating by Direct Sunlight

The contribution of direct sunlight is the main source of heat energy and therefore a critical part of the simulation.

The total amount of solar heat energy received by a triangle depends on the total solar irradiation, which varies during the year because of the eccentricity of earth's orbit, the orientation of the triangle to the sun, atmospheric influences, and whether the triangle is actually irradiated by the sun or shaded.

The solar irradiation outside of the atmosphere for a surface directly faced to the sun can be approximated by

$$E_{\text{total}} = 1367(1 + 0.033 \cos(2\pi n/365)),$$

where n denotes the day of year, cf. (Maréchal et al., 2010). The fraction of the area facing the sun is calculated from the sun direction \mathbf{s} and the normal of the surface \mathbf{n}_s by $\cos(\varphi) = \mathbf{s} \cdot \mathbf{n}_s$, where φ denotes the angle between the sun ray and surface normal. The solar irradiance before atmospheric filtering is given by

$$E_{\text{Sun}} = E_{\text{total}} \cdot \cos(\varphi).$$

The atmosphere absorbs solar radiation, which is modeled by weighting the sun irradiance with the clearness factor I_c . Furthermore, a fraction of the irradiance is not absorbed by the surface, but reflected back. This effect is represented by the albedo of the surface which depends on the color and material property of the triangle, yielding to the solar irradiance

$$\tilde{S} = (1 - \alpha)I_c E_{\text{Sun}} \cos(\theta), \quad (27)$$

where θ is the sun's elevation angle. If the triangle is actually illuminated by the sun or occluded by other triangles is stated by a factor $\gamma_{\text{Sun}} \in \{0, 1\}$ which is determined using an OpenGL rendering of the scene analogous to 3.2.4. More precisely, an index image of the scene from the viewpoint of the sun is rendered, then γ_{Sun} is set to 1 if the triangle is visible on the rendered picture or 0 otherwise. This allows to deal with thermal shadows in the simulation. In summary, the solar irradiation on the surface is given by

$$S = (1 - \alpha)I_c E_{\text{Sun}} \cos(\theta) \gamma_{\text{Sun}}. \quad (28)$$

4 RESULTS

In this section, the results for two data sets are presented. The method was implemented in MATLAB with the parallel processing toolbox on an Intel(R) I7-8700 3.19GHz CPU with 32GB RAM and NVIDIA GeForce GTX 1080 GPU. The first data set represents

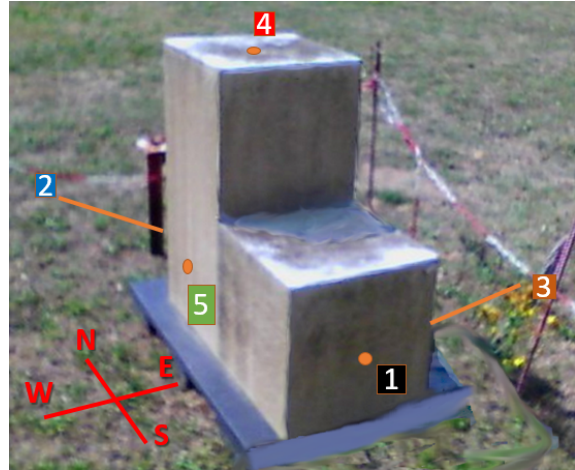


Figure 4: CUBI in Ettlingen with five thermistors (south, north, east, top, west).

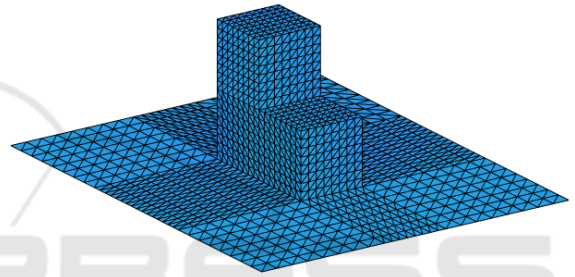


Figure 5: Watertight CUBI and Ground mesh with 2816 triangles.

a simple scene with known ground truth; hence it can be used for validation. The second data set consists of various sensor data of an urban area, so we used the proposed four-step pipeline and compared the result of the thermal simulation with a thermal image.

4.1 CUBI – Thermal Model Validation

CUBI is a simple geometrical object used in outdoor experiments to collect data for testing and validation of thermal models and infrared imaging. It has the shape of a stair, like three compound cubes with an edge length of 0.5m. For the validation of our thermal model, we use the data of (Malaplate et al., 2007) that include time series of different surface temperature acquired by thermistors in Ettlingen, Germany, in May 2006. In Figure 4, the CUBI test object with the positions of thermistors is shown.

Representing the geometry of CUBI and the ground, a mesh with 2816 triangles was created, as shown in Figure 5.

As material parameters for the CUBI as well as for the ground, we use those for metal, retrieved from the material database. For the inner model, 10 layers are

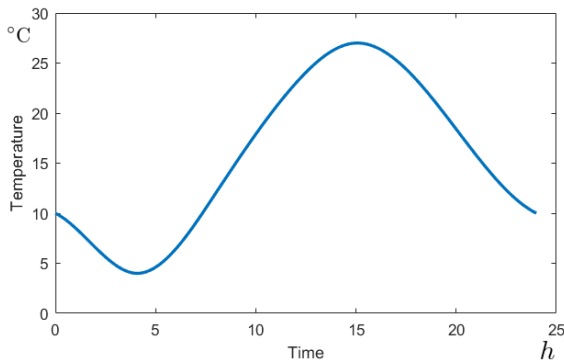


Figure 6: Simplified air temperature curve used for simulation.

used with a thickness of $0.1m$.

We simulate a two-days cycle from 2006-05-11 to 2006-05-12 for the location of Ettlingen 48;56;48 N 8;24;38E with a simplified air temperature curve shown in Figure 6. We use the same air temperature curve for both days with a minimum temperature of $4^{\circ}C$ at 4:00 am and a maximum temperature of $27^{\circ}C$ at 3:00 pm.

Figure 7 shows the temperature distribution of the CUBI at 1:00 pm. The thermal shadow of the CUBI is recognizable by the blue color on the ground on the right part of the picture. The heat conduction is also clearly visible as color gradient at the shadow and at the edges of surfaces, for those one surface is in the shade and the other is illuminated by the sun.

In Figure 8 the collected and simulated data of the thermistors is shown. Both curves show a good qualitative agreement: The order of the peaks is identical. As expected, the eastern thermistor (brown/yellow) reaches its maximum at about 10 o'clock and then cools down in a similar way until evening, i.e. both curves show a small hump. Also the maximum temperature is about the same at $40^{\circ}C$. The upper and southern thermistors (red and black) reach their maximum at about 12 o'clock, which corresponds to the measured data, the temperature is only slightly overestimated in the simulation. Finally, the western thermistor reaches its maximum in the evening, which is slightly underestimated compared to the measured data. The northern thermistor (blue) is also underestimated in the simulation. One reason for this could be inaccuracies in the inner model. Since the CUBI is a relatively small object, the assumption that the internal temperature is constant may be inaccurate.

In conclusion, the thermal model provides good results for simple geometries.

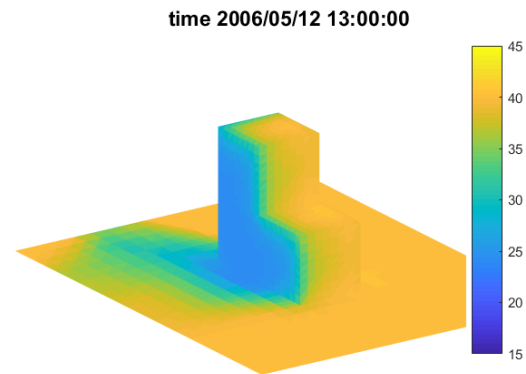


Figure 7: Simulated temperature distribution of CUBI on 2006-05-12 at 1pm in Ettlingen in $^{\circ}C$.

4.2 Melville – Thermal Simulation for Large Sceneries

Our second data set is provided by the City of Melville, a local council located in Perth, Australia. This council aims at sustainable and energy-efficient urban development, for which, among others, studies investigating the influence of land usage on heat islands are being carried out, see (Council of City of Meville, 2017). For this purpose, heterogeneous airborne sensor data, such as multispectral imagery, a thermal infrared image and a LiDAR point cloud as well as seven-years-old shapefile containing building outlines were available from the eponymous town. We selected a residential area measuring $1\text{ km} \times 2\text{ km}$ and containing some 1500 buildings and many trees. After all data was registered into the same coordinate system, the steps mentioned in Section 2.2 were applied. Note that we used the sensor data for classification while we generated LoD0 building objects from the building footprints contained in the shapefiles (Biljecki et al., 2016). We have not considered it as a severe drawback that the shapefile was outdated in some areas, since our main task here is to prove the capability of the approach to simulate large scenes. Moreover, those larger parts of the terrain that were classified as buildings but not listed in the shapefile were modeled as brick.

Considering the material classes needed for the thermal simulation, we restrict ourselves to the ones given in Table 2 where ground cover classes are related to the ground mesh only. Each semantic class has been assigned: material parameters as listed in Table 1, a specific core temperature, and a free convection coefficient dependent on the environment (i.e. the convective medium) and the material. Concerning 3D objects, we consider buildings and forest boxes.

In Figure 9, a detail of the city of Melville is shown together with our classification and triangula-

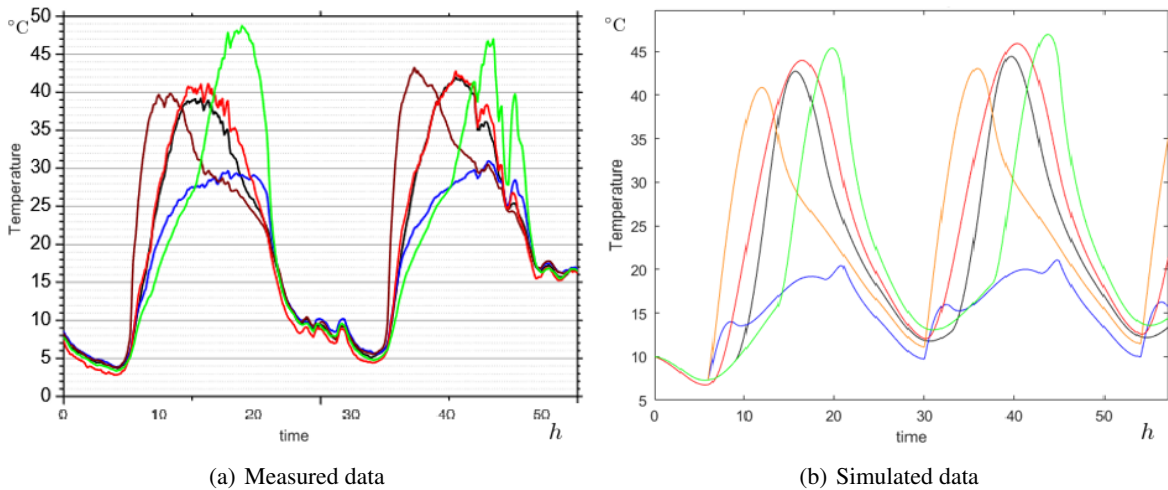
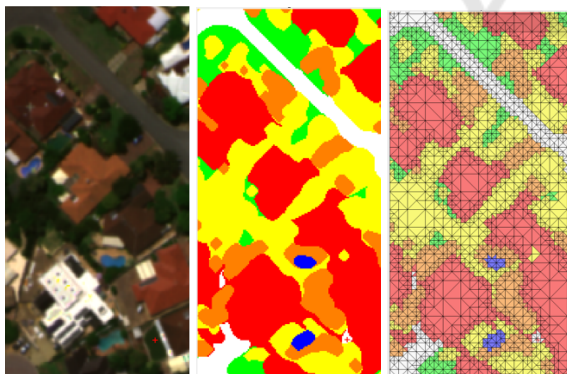


Figure 8: Measured and simulated temperatures for May 11 and 12, 2006, for thermistors 1 (black), 2 (blue), 3 (yellow), 4 (red) and 5 (green).

Table 2: Material classes of Melville data set.

	Semantic Class	color
Ground cover	Street	white
	Soil	orange
	Grass	green
	Brick	red
	Tree	yellow
	Water	blue
3D Object	Building wall	
	Roof	
	Forest box wall	
	Forest box roof	



(a) RGB-Image (b) Classification (see Table 2) (c) RTDQT

Figure 9: Generation of terrain mesh.

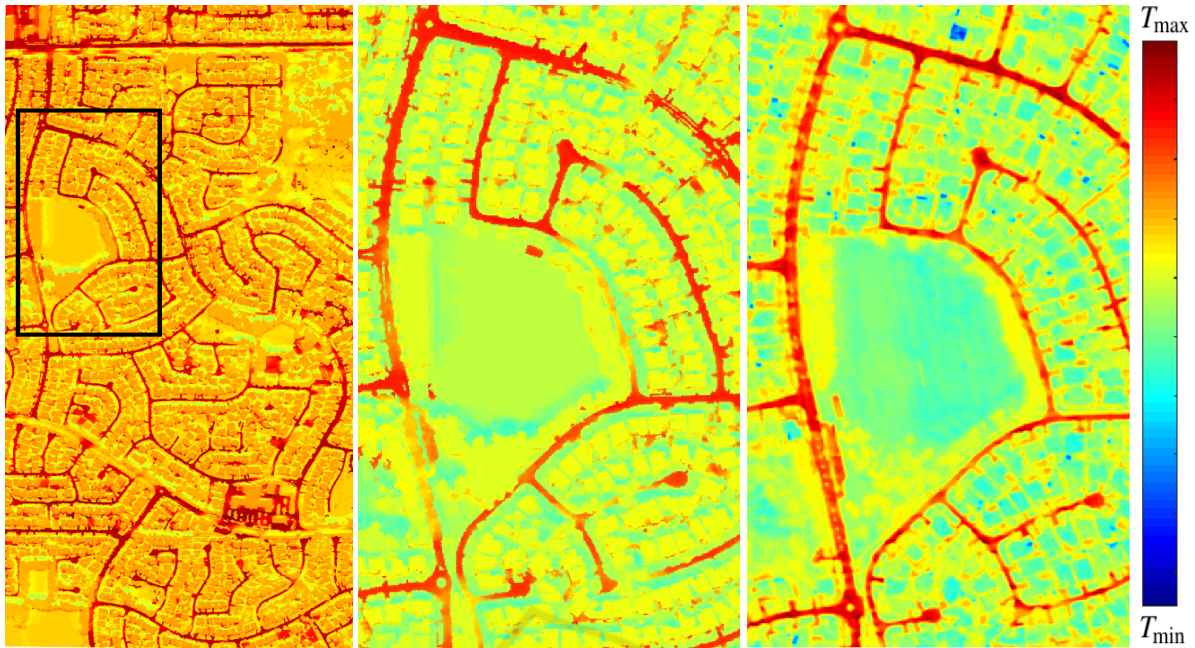
tion result of the ground.

In the simulation presented in the following, we have chosen the forced convection to be neglected by setting the wind velocity to zero, i.e. regarding a windless scene. As further weather condi-

tions, we used the same as for the CUBI scenario. The whole scene consists of 1313410 triangles, and 706405 points and 10 sets of material parameters. The simulation terminated in 252 sec. for five day-night cycles.

Figure 10 (a) shows our simulation result, i.e. the resulting surface temperatures of the city of Melville at the time 7h00 on a day in September. The structure of the city is clearly visible and the different thermal behaviour of the materials appears realistic: the streets are visible as warm areas and the areas with vegetation are cooler. Figure 11 shows the surface temperatures of the scene at noon in a slanted view, so that the 3D structure becomes visible. Here, the effect of thermal shadows is demonstrated. They are visible on surfaces which are not illuminated by the sun and therefore are exposed to less heating, i.e. the surface temperature is cooler.

The thermal image of the city of Melville results from several measurements during night time and allows a first comparison between our simulation result and actual sensor data. Figures 10(b) shows a smaller region of our simulation result at nighttime and Figure 10(c) the corresponding thermal image. In direct comparison, our heat simulation shows good agreement with the thermal image. We have successfully reproduced the strong signature of the streets during night and the cooling effect by trees on the streets, which can punctually be seen along the long road on the left side of both images. Merging several trees and modeling them as forest boxes proves to be convenient, e.g. the surrounding tree areas around the large grass field return a reasonable surface temperature. Differences between simulation and the thermal image appear considering effects by shadow cast.



(a) Simulation result (topview) for the city of Melville at 7h00 (b) Simulated Surface Temperatures (c) Thermal Infrared Image

Figure 10: Comparison between simulated temperatures and thermal infrared image.

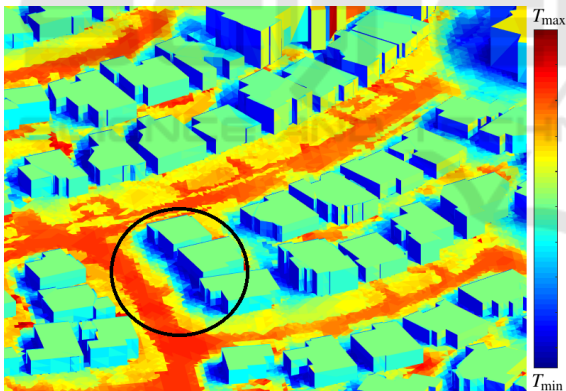


Figure 11: Slanting view on the simulation results for the city of Melville at noon. Areas not directly exposed to sunlight heat up less and generate thermal shadows (circle).

Within the simulation, shadow casts lead to strong cooling which is not present in the thermal sensor image. Furthermore, building roofs show a considerably lower temperature than in the simulation. We suspect that this is due to the material properties, in particular a low emissivity, which makes objects appear cooler on thermal images than they actually are. Field measurements might give more information about the actual roofing temperatures to enable an evaluation of these differences.

5 CONCLUSIONS

In this paper, we have presented a thermal simulation approach for large scenes in the framework of a pipeline leading from raw sensor data to 3D environments rendered in the infrared spectrum. The preceding work of the thermal simulation consists of the material classification and mesh generation from the sensor data. Given the triangulation, we define a surface volume as simulation element for discretization of the heat transfer equation. Our model results in qualitatively good agreement between simulation and ground truth data for small geometries such as the CUBI object. Applied to a large data set using the entire pipeline up to thermal simulation, we have shown that our method efficiently leads to similar surface temperatures as compared to a thermal image. Outstanding signatures in the thermal image are recognizable in the simulation at a comparable point in time. Furthermore, the simulation with time displays the dependency of the solar irradiation and the resulting thermal shadows as we expected. Completing the pipeline towards infrared rendering, where the heat radiance is modeled, will lead to an optimized starting point for comparison between thermal imaging and simulation. Also, modeling the heat radiation in future work will be a promising tool for urban heat island consideration and other applications.

ACKNOWLEDGEMENTS

We express our deep gratitude to the City of Melville and Dr. Petra Helmholz from Curtin University, Australia, for the acquisition of the Melville data set as well as Rebecca Ilehag from Karlsruhe Institute of Technology, Germany, for data preparation. We thank our colleagues Jonas Mispelhorn for providing the OpenGL renderer and Dr. Jochen Meidow for reading parts of the manuscript.

REFERENCES

- Bartos, B. and Stein, K. (2015). FTOM-2D: a two-dimensional approach to model the detailed thermal behavior of nonplanar surfaces. In *Target and Background Signatures*, volume 9653, page 96530G. International Society for Optics and Photonics.
- Biljecki, F., Ledoux, H., and Stoter, J. (2016). An improved LoD specification for 3D building models. *Computers, Environment and Urban Systems*, 59:25–37.
- Breiman, L. (2001). Random forests. *Machine learning*, 45(1):5–32.
- Bulatov, D., Häufel, G., Meidow, J., Pohl, M., Solbrig, P., and Wernerus, P. (2014). Context-based automatic reconstruction and texturing of 3D urban terrain for quick-response tasks. *ISPRS Journal of Photogrammetry and Remote Sensing*, 93:157–170.
- Council of City of Meville (2017). Urban forest strategic plan 2017-2036: Plan a: City-controlled plan. Technical report, City of Melville, Perth, Australia.
- Decaudin, P. and Neyret, F. (2004). Rendering forest scenes in real-time. In *EGSR04: 15th Eurographics Symposium on Rendering*, pages 93–102. Eurographics Association.
- Dewan, A. M. and Corner, R. J. (2014). Impact of land use and land cover changes on urban land surface temperature. In *Dhaka Megacity*, pages 219–238. Springer.
- Feng, X. and Myint, S. W. (2016). Exploring the effect of neighboring land cover pattern on land surface temperature of central building objects. *Building and Environment*, 95:346–354.
- Gross, H. and Thönnessen, U. (2006). Extraction of lines from laser point clouds. *International Archives of Photogrammetry, Remote Sensing and Spatial Information Sciences*, 36 (Part 3/W49):86–91.
- Häufel, G., Bulatov, D., and Solbrig, P. (2017). Sensor data fusion for textured reconstruction and virtual representation of alpine scenes. In *Earth Resources and Environmental Remote Sensing/GIS Applications VIII*, volume 10428, page 1042805. International Society for Optics and Photonics.
- Ilehag, R., Bulatov, D., Helmholz, P., and Belton, D. (2018). Classification and representation of commonly used roofing material using multisensorial aerial data. *International Archives of the Photogrammetry, Remote Sensing & Spatial Information Sciences*, 42(1).
- Johnson, K., Curran, A., Less, D., Levanen, D., Marttila, E., Gonda, T., and Jones, J. (1998). MuSES: A new heat and signature management design tool for virtual prototyping. In *Proc. of the 9th Annual Ground Target Modelling and Validation Conference*.
- Kajiya, J. T. (1986). The Rendering Equation. In *Proc. of the 13th Annual Conference on Computer Graphics and Interactive Techniques*, SIGGRAPH '86.
- Lagouarde, J.-P., Hénon, A., Kurz, B., Moreau, P., Irvine, M., Voogt, J., and Mestayer, P. (2010). Modelling daytime thermal infrared directional anisotropy over toulouse city centre. *Remote Sensing of Environment*, 114(1):87–105.
- Lienhard IV, J. H. and Lienhard V, J. H. (2011). *A heat transfer textbook*. Dover Publ., Mineola, NY, 4. ed., corr., rev. and updated edition.
- Malaplate, A., Grossmann, P., and Schwenger, F. (2007). Cubi: a test body for thermal object model validation. In *Infrared Imaging Systems: Design, Analysis, Modeling, and Testing XVIII*, volume 6543, page 654305. International Society for Optics and Photonics.
- Maréchal, N., Guérin, E., Galin, E., Mérillou, S., and Mérillou, N. (2010). Heat transfer simulation for modeling realistic winter sceneries. In *Computer Graphics Forum*, volume 29, pages 449–458. Wiley Online Library.
- Pajarola, R. (2002). Overview of quadtree-based terrain triangulation and visualization. Technical report, Department of Information & Computer Science, University of California, Irvine.
- Poglio, T., Savaria, E., and Wald, L. (2002). Outdoor scene synthesis in the infrared range for remote sensing applications. In *CISST'02: International Conference on Imaging Science, Systems, and Technology*. CSREA Press, Athens, Ga, USA.
- Siegel, R. and Howell, J. R. (1992). *Thermal radiation heat transfer*. Francis & Taylor, Washington, DC, 3. ed. edition.
- Sonntag, D. (1990). Import new values of the physical constants of 1986, vapour pressure formulations based on the ITS-90, and psychrometer formulae. *Z. Meteorol*, 70:340.
- Xiong, B., Elberink, S. O., and Vosselman, G. (2014). Building modeling from noisy photogrammetric point clouds. *ISPRS Annals of the Photogrammetry, Remote Sensing and Spatial Information Sciences*, 2(3):197–204.
- Xiong, X., Zhou, F., Bai, X., Xue, B., and Sun, C. (2016). Semi-automated infrared simulation on real urban scenes based on multi-view images. *Optics Express*, 24(11):11345–11375.